JOURNAL OF GEOPHYSICAL RESEARCH, VOL. 87, NO. B11, PAGES 9317-9328, NOVEMBER 10, 1982

# Theory of the Development of Geothermal Systems Charged by Vertical Faults

G. S. BODVARSSON, S. M. BENSON, AND P. A. WITHERSPOON

*Earth Sciences Division, Lawrence Berkeley Laboratory, Berkeley, California 94720*

A two-dimensional model of fault-charged hydrothermal systems has been developed that considers the transient development of such systems including the effects of heat losses to the confining layers. The model can be used for theoretical studies of the development of fault-charged reservoirs. It can also be used to estimate the rate of recharge from the fault source and the time of evolution, using temperature data from wells. The model has been applied to the hydrothermal system at Susanville, California. A reasonable match with the areal temperature distribution in the primary aquifer and the temperature profiles of individual wells was obtained. This allowed an estimate of the recharge rate from the fault into the hydrothermal system to be obtained. As the calculated recharge rate ($9 \times 10^{-6}$ $m^3/s$ m) into the Susanville hydrothermal system proved to be quite significant, a threefold increase in the potential of the Susanville hydrothermal anomaly for space heating purposes is predicted.

## INTRODUCTION

The development of geothermal systems and the factors that control their development are matters of considerable interest. Thermally induced natural convection is one of the most effective means of transferring mass and energy through rock layers, and this phenomenon has been investigated by many workers. However, not as much attention has been given to the development of fault-charged geothermal systems. Fault-charged reservoirs are those where one or more major faults provide most of the energy to the geothermal reservoir.

Fault-charged reservoirs commonly display atypical temperature profiles that are characterized by a reversal (Figure 1). The profiles are indicative of lateral hot water flow and conductive heat losses to the confining beds. These temperature data can be analyzed to yield the recharge rate into the hydrothermal system and its time of evolution.

Fault-charged geothermal systems are found in most geothermally active areas in the world. Examples of such systems in the western part of the United States are the high temperature fields such as Roosevelt Hot Springs, Utah, and East Mesa in Imperial Valley, California. Low-moderate temperature systems of this type include Klamath Falls and Vale in Oregon and the Susanville hydrothermal system in California.

The distinct characteristics of fault-charged geothermal systems make it necessary to develop a theoretical basis for understanding their evolution and their behavior under exploitation. In this paper a new model for analyzing fault-charged geothermal systems is presented. As will be illustrated, the model provides some important new insights into the factors that control the development and behavior of such systems. Finally, application of the model, using data from the Susanville, California, hydrothermal system, is illustrated.

## GENERAL BACKGROUND

Several studies on fault-charged reservoirs have appeared in the literature. *Sorey* [1975] used a numerical simulator to study heat losses associated with a hot spring system. He considered two models, a cylindrical fault zone and a linear fault discharging hot water from depth into a hot spring. Generally, the rock formation around the faults was assumed impermeable so that heat losses from the fault are only due to conduction. By varying the geometrical dimensions of the problem and the discharge rate, he calculated the steady state temperature distribution around the fault and the temperature of the discharged fluids at the hot spring.

*Pritchett and Garg* [1979] used numerical techniques to calculate the transient thermal and velocity fields in a fault-charged aquifer. Heat transfer associated with fluid flow up the fault was neglected, but they modeled in reasonable detail the mass and heat transport within the aquifer. Heat losses to the caprock were approximated by a quasi-steady state process, while heat losses to the bedrock were neglected. *Kilty et al.* [1978] developed a finite difference numerical model to study convective heat transfer in geothermal systems. In their model the flow field was assumed a priori, and the steady state convective and conductive heat transfer was then calculated. They applied the model to the Monroe, Utah, hydrothermal system and studied the temperature distribution in the system caused by steady upflow of water in a vertical fault.

*Riney et al.* [1979] used a numerical model to study the temperature distribution at the East Mesa hydrothermal system in the Imperial Valley of California. They assumed that the reservoir is recharged by a cylindrical fault system, representing the intersection of three major faults. They modeled the mass and heat transfer in the aquifer in some detail, but used only an approximate representation of heat losses to the caprock and neglected heat losses to the bedrock altogether. They obtained a reasonable match with the steady state temperature distribution in the reservoir and heat flow at the surface. However, the authors recognized the non-uniqueness of the reservoir parameters obtained, especially the porosities and permeabilities in the reservoir.

Using a semi-analytic approach, *Goyal and Kassoy* [1980] developed a steady state model of a fault-charged reservoir system. They specified the flow rate and the temperature of the fluids in the fault at the bottom of the reservoir. Vertical flow within the reservoir was neglected. Constant temperature boundary conditions at the top and bottom of the reservoir were prescribed in their model. *Goyal and Kassoy*



Paper number 2B1205.

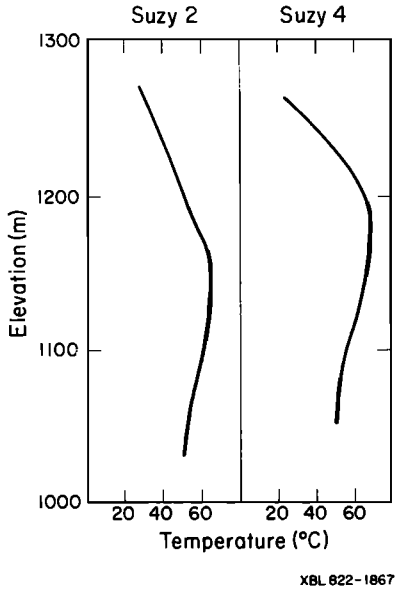


Fig. 1. Example of typical temperature profiles from two wells in a fault-charged reservoir (Susanville, California).

[1981] applied the model to the East Mesa hydrothermal system. They calculated the recharge rate to the fault, vertical variations of horizontal velocities within the aquifer, temperature fields in the aquifer and caprock, and surface heat flows. A reasonable qualitative match with observed data from the field was obtained, but some quantitative differences in the temperature field and the surface heatflows still remained. *Goyal and Narasimhan* [1981] have recently used a similar model for a constant pressure charging of a fault-controlled geothermal reservoir.

The model to be presented here is fully transient and includes conductive heat transfer to the caprock and bedrock. Vertical variations in temperature and velocity within the aquifer are ignored. Therefore, our model is most applicable to relatively thin aquifer systems and can be used to study the evolution of such systems as well as their steady state behavior.

## Mathematical Model

Figure 2 shows the fault-charged geothermal system for which a mathematical model has been developed. Initially, temperatures increase linearly with depth with a geothermal gradient, $a$. At time $t = 0$, hot water starts to flow up the vertical fault and is recharged into a relatively thin horizontal aquifer under forced convection. The behavior of the system is then controlled by the following assumed conditions:

1. At the ground surface, the temperature, $T_{b1}$, remains constant.
2. No heat losses occur as the fluid moves up the fault and enters the aquifer at a constant temperature $T_f$. This assumption is commonly made in the analysis of fault-charged systems and will result in some errors in the temperature field close to the fault.
3. Within the aquifer (1) the mass flow rate is constant, (2) horizontal conduction is neglected, (3) temperatures in the vertical direction across the relatively thin aquifer are uniform, and (4) thermal equilibrium between fluid and solid is instantaneous.
4. Within the confining beds (caprock and bedrock) (1) the permeability is so low that movement of heat is controlled only by heat conduction, (2) horizontal conduction is neglected (numerical studies by *Bodvarsson and Tsang* [1982]) have shown that this assumption is quite reasonable, (3) there is no resistance to heat transfer at the interfaces with the aquifer.
5. At some depth, $B$, below the aquifer, the temperature in the bedrock, $T_{b2}$, is constant.
6. The thermal properties of the formations above and below the aquifer may be different, but all thermal parameters for the liquid and rock are constant.

Based on the above assumptions, the differential equation governing the temperature in the aquifer at any time $t$ can readily be derived by performing an energy balance on a control volume in the aquifer:

$$z = 0: \frac{\lambda_1}{H}\frac{\partial T_1}{\partial z}\bigg|_{z=0} - \frac{\lambda_2}{H}\frac{\partial T_2}{\partial z}\bigg|_{z=0} - \frac{\rho_w c_w q}{H}\frac{\partial T_a}{\partial x} - \rho_a c_a \frac{\partial T_a}{\partial t} = 0 \quad (1)$$

Similar equations for different systems have been derived by *Lauwerier* [1955], *Bodvarsson* [1972], *Bodvarsson and Tsang* [1982], and others. In the caprock and bedrock, temperatures are controlled by the one-dimensional, heat-conduction equation

$$z > 0: \quad \lambda_1 \frac{\partial^2 T_1}{\partial z^2} = \rho_1 c_1 \frac{\partial T_1}{\partial t} \quad (2)$$

$$z < 0: \quad \lambda_2 \frac{\partial^2 T_2}{\partial z^2} = \rho_2 c_2 \frac{\partial T_2}{\partial t} \quad (3)$$

The initial conditions are

$$T_a(x, 0) = T_{b1} + a_1 D \quad (4a)$$

$$T_1(x, z, 0) = T_{b1} - a_1(z - D) \quad (4b)$$

$$T_2(x, z, 0) = T_{b1} + a_1 D - a_2 z \quad (4c)$$

The boundary conditions are

$$T_a(0, t) = T_f \qquad t > 0 \quad (5a)$$

$$T_a(x, t) = T_1(x, 0, t) = T_2(x, 0, t) \quad (5b)$$

$$T_1(x, D, t) = T_{b1} \quad (5c)$$

$$T_2(x, -B, t) = T_{b2} = T_{b1} + a_1 D + a_2 B \quad (5d)$$

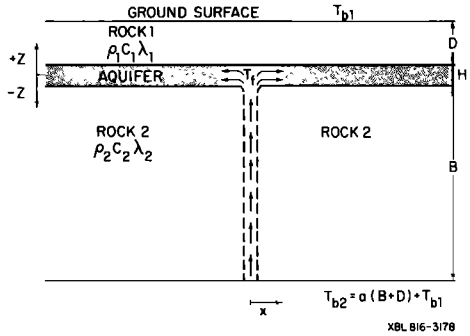


Fig. 2. The mathematical model considered for fault problem.

The following dimensionless parameters are introduced:

Dimensionless distance

$$\xi_1 = \frac{\lambda_1 x}{\rho_w c_w q D} \tag{6a}$$

Dimensionless time

$$\tau_1 = \frac{\lambda_1 t}{\rho_1 c_1 D^2} \tag{6b}$$

Dimensionless energy potential

$$\theta_1 = \frac{H}{D}\frac{\rho_a c_a}{\rho_1 c_1} \tag{6c}$$

Dimensionless vertical coordinate

$$\eta = \frac{z}{D} \tag{6d}$$

Heat capacity ratio

$$\gamma = \frac{\rho_2 c_2}{\rho_1 c_1} \tag{6e}$$

Thermal conductivity ratio

$$\kappa = \frac{\lambda_2}{\lambda_1} \tag{6f}$$

Dimensionless temperature

$$T_D = \frac{T - T_{b1}}{T_f - T_{b1}} \tag{6g}$$

Dimensionless thermal gradient

$$T_g = \frac{a_1 D}{T_f - T_{b1}} \tag{6h}$$

Geometrical factor

$$\sigma = \frac{B}{D} \tag{6i}$$

Geothermal gradient ratio

$$\omega = \frac{a_2}{a_1} \tag{6j}$$

After introducing equations (6a)–(6j), equations (1)–(3) become

$$\eta = 0: \left.\frac{\partial T_{D_1}}{\partial \eta}\right|_{\eta=0} - \kappa \left.\frac{\partial T_{D_2}}{\partial \eta}\right|_{\eta=0} - \frac{\partial T_{D_a}}{\partial \xi_1} - \theta_1 \frac{\partial T_{D_a}}{\partial \tau_1} = 0 \tag{7}$$

$$\eta > 0: \frac{\partial^2 T_{D_1}}{\partial \eta^2} = \frac{\partial T_{D_1}}{\partial \tau_1} \tag{8}$$

$$\eta < 0: \frac{\partial^2 T_{D_2}}{\partial \eta^2} = \frac{\gamma}{\kappa}\frac{\partial T_{D_2}}{\partial \tau_1} \tag{9}$$

The initial condition (equation (4)) becomes

$$T_{D_a}(\xi_1, 0) = T_g \tag{10a}$$

$$T_{D_1}(\xi_1, \eta, 0) = -T_g(\eta - 1) \tag{10b}$$

$$T_{D_2}(\xi_1, \eta, 0) = -T_g(\omega\eta - 1) \tag{10c}$$

The boundary conditions (equations (5a)–(5d)) become

$$T_{D_a}(0, \tau_1) = 1 \qquad \tau_1 \geq 0 \tag{11a}$$

$$T_{D_a}(\xi_1, \tau_1) = T_{D_1}(\xi_1, 0, \tau_1) = T_{D_2}(\xi_1, 0, \tau_1) \tag{11b}$$

$$T_{D_1}(\xi_1, 1, \tau_1) = 0 \tag{11c}$$

$$T_{D_2}(\xi_1, -\sigma, \tau_1) = T_g(\omega\sigma + 1) \tag{11d}$$

Solutions to equations (7)–(11) can be obtained in the Laplace domain (see Appendix 1) as the following set:

$$\eta = 0: u = \frac{1}{p}[1 - T_g] \exp - \left[\theta_1 p + \frac{\sqrt{p}}{\tanh\sqrt{p}} + \frac{\kappa\sqrt{(\gamma/\kappa)p}}{\tanh \sigma\sqrt{(\gamma/\kappa)p}}\right]\xi_1 + \frac{T_g}{p} \tag{12}$$

$$\eta > 0: v_1 = \left[u - \frac{T_g}{p}\right]\cosh\sqrt{p}\eta - \frac{\left[u - \frac{T_g}{p}\right]}{\tanh\sqrt{p}}\sinh\sqrt{p}\eta - \frac{T_g}{p}(\eta - 1) \tag{13}$$

$$\eta < 0: v_2 = \left[u - \frac{T_g}{p}\right]\cosh\sqrt{\frac{\gamma}{\kappa}p}\,\eta + \frac{\left[u - \frac{T_g}{p}\right]}{\tanh \sigma\sqrt{(\gamma p/\kappa)}}\sinh\sqrt{(\gamma p/\kappa)}\eta - \frac{T_g}{p}(\omega\eta - 1) \tag{14}$$

In equations (12)–(14), $u$ and $v$ represent the temperatures in the Laplace domain for the aquifer and the confining layers, respectively. Although closed form asymptotic solutions to these equations may be obtained, the complete solution cannot easily be inverted from the Laplace domain. A numerical scheme developed by *Stehfest* [1970] was therefore used to obtain the results to be presented below.

### *Validation of Present Model*

As a check on the validity of our mathematical model, we compared our work with that of *Lauwerier* [1955]. Lauwerier considered lateral flow in an aquifer bounded by vertically infinite confining layers. At intermediate times, before the influence of constant temperature boundaries at $z = D$, and $z = -(B + D)$ are felt, our solution for the aquifer (equation (12)) should be identical with that of Lauwerier, provided (1) there is no geothermal gradient, i.e., $a = 0$, and (2) the thermal properties in the caprock and the bedrock are the same, i.e., $\gamma = \kappa = 1.0$.

The Lauwerier solution is thus a special case of the present solution. Figure 3 shows a comparison between our

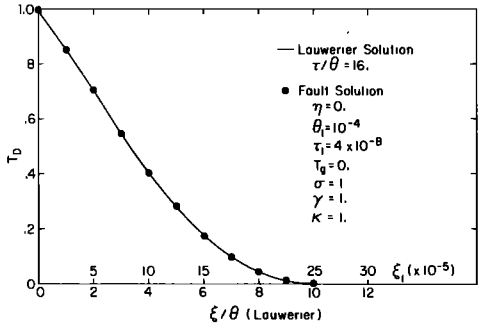


Fig. 3. Comparison between the present solution and the Lauwerier solution.

solution for temperature distribution in the aquifer and the Lauwerier solution for a given set of parameters. Note that in Figure 3 the parameters $\tau$, $\xi$, and $\theta$ are as defined by Lauwerier; all other parameters are defined in the nomenclature. The match between our solution and that of Lauwerier is near-perfect, confirming the validity of the present model.

*Asymptotic Solutions*

At early times, the solution for the temperature in the aquifer simplifies considerably, so that inversion into real space is possible (see Appendix 2). The solution in real space is

$$T_{D_a} = [1 - T_g]U[\tau_1 - \theta_1\xi_1] + T_g \tag{15}$$

where $U$ denotes the unit step function. Equation (15) shows that when the dimensionless time $\tau_1$ is less than $\theta_1\xi_1$, the initial temperature $T_g$ prevails. However, in the thermal region, when $\tau_1$ is greater than $\theta_1\xi_1$, the aquifer temperature equals the temperature of the fault water. No temperature changes occur in the caprock and the bedrock at early times.

At late times the solutions for the temperatures in the Laplace domain (equations (12)–(14)) also simplify to the extent that inversion to real space is possible. In real space the steady state solutions are (see Appendix 2)

$$\eta = 0\text{: } T_{D_a} = [1 - T_g] \exp - \left[1 + \frac{\kappa}{\sigma}\right]\xi_1 + T_g \tag{16}$$

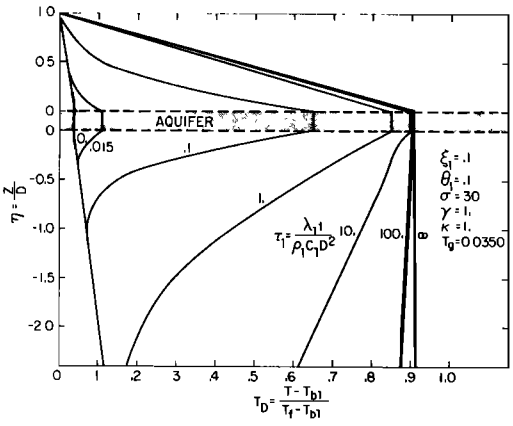


Fig. 4. Evolution of a fault-charged hydrothermal system for $\xi_1 = 0.1$.

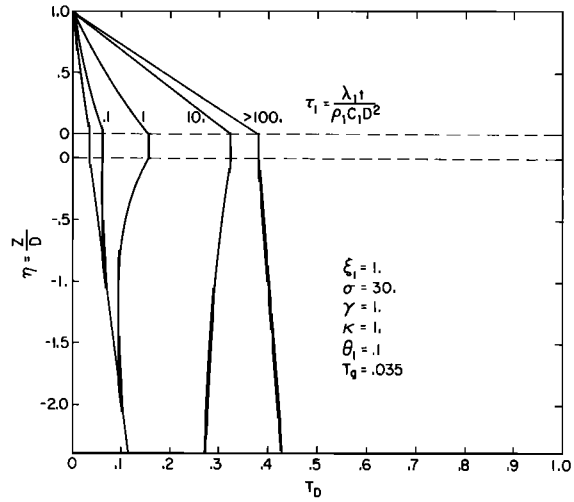


Fig. 5. Evolution of a fault-charged hydrothermal system for $\xi_1 = 1.0$.

$$\eta > 0\text{: } T_{D_1} = [1 - T_g][1 - \eta] \exp - \left[1 + \frac{\kappa}{\sigma}\right]\xi_1 - T_g(\eta - 1) \tag{17}$$

$$\eta < 0\text{: } T_{D_2} = [1 - T_g]\left[1 + \frac{\eta}{\sigma}\right] \exp - \left[1 + \frac{\kappa}{\sigma}\right]\xi_1 - T_g(\omega\eta - 1) \tag{18}$$

Equations (16)–(18) show that the steady state temperature profiles are independent of $\theta_1$, as well as the heat capacity ratio ($\gamma$).

## Evolution of Fault-Charged Hydrothermal Systems

The model has been employed to study the evolution of fault-charged hydrothermal systems. Figure 4 shows a plot of dimensionless temperature $T_D$ versus depth at a given location for several different values of dimensionless time $\tau_1$. Initially ($\tau_1 = 0$) the system is in equilibrium with a linear geothermal gradient, and hot water starts to flow into the permeable aquifer. In the early stages of development, only the aquifer is being heated. Later on, however, conductive heat transfer between the aquifer and the adjacent rocks increases, causing the caprock and bedrock to be heated and temperatures in the aquifer to stabilize.

Temperatures in the aquifer and caprock reach steady state at a dimensionless time $\tau$, between 1 and 10. However, at this time the temperatures in the rock formation below the aquifer are not yet near steady state. This is a consequence of the high value of $\sigma = 30$. Since the constant-temperature boundary at the ground surface is much closer to the aquifer than the deep boundary, this is the factor that controls the thermal response. Note that the steady state temperature in the aquifer at the location in question is approximately $T_D = 0.91$.

Further away from the fault one would anticipate a similar behavior with less temperature rise. Figure 5 shows the thermal evolution at the dimensionless distance from the

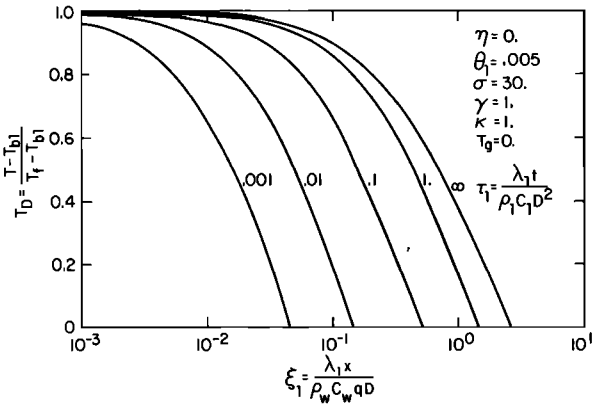


Fig. 6. Evolution of the thermal field in the aquifer.

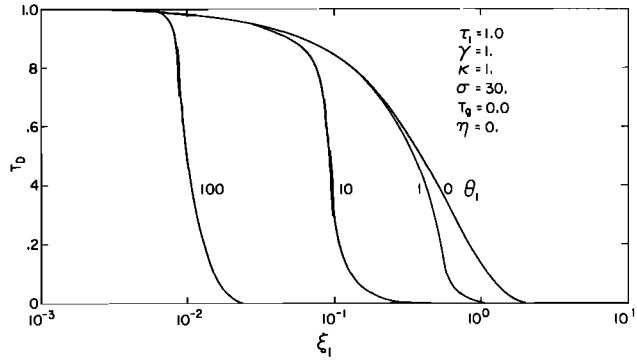


Fig. 7. $\theta_1$-dependence of the temperature profile along the aquifer for $\tau_1 = 1.0$.

fault of $\xi_1 = 1.0$. Note that the steady state dimensionless temperature in the aquifer is only about $T_D = 0.4$, or less than half that attained for a dimensionless distance of $\xi_1 = 0.1$. Consequently, the temperature gradient in the caprock is also reduced. Obviously, closer to the fault, where $\xi_1 < 0.1$, the aquifer will be heated more fully to temperatures that are essentially $T_D = 1.0$.

*Evolution of Thermal Field Within the Aquifer*

Figure 6 shows the evolution of the thermal field within the aquifer for $\theta_1 = 0.005$ and other parameters as specified in the figure. It shows that close to the fault (small $\xi_1$) the temperature rises almost immediately to the temperature of the recharging water. The figure also shows that a steady state thermal field is reached shortly after dimensionless time $\tau_1$ exceeds 1.0. Although the steady state thermal field is independent of $\theta_1$ (see equations (16)–(18)), the transient development of the thermal field is greatly affected by $\theta_1$. This is illustrated in Figure 7 for $\tau = 1.0$, where it may be seen that the smaller $\theta_1$ is, the further away from the fault the thermal front has advanced. This is reasonable since $\theta_1$ represents the heat capacity of the aquifer normalized to that of the caprock. Thus, the higher the value of $\theta_1$ the greater the heat capacity of the aquifer and consequently smaller volume of the aquifer away from the fault becomes heated. Figure 7 also shows that for higher values of $\theta_1$, the location of the thermal front ($T_D = 0.50$) can be expressed by the simple relation,

$$\tau_1 = \theta_1 \xi_1 \tag{19}$$

It is apparent that, for values of $\theta_1$ below 10, equation (19) no longer holds.

Low values of $\theta_1$ imply low aquifer heat capacity, and, consequently, significant heat conduction losses to the caprock and bedrock will occur. We found this to be the case for values of dimensionless times ranging up to $\tau_1 = 1.0$.

*Heat Losses From the Aquifer*

Heat losses from the aquifer to the caprock and bedrock can be calculated at any given time by the Fourier law of heat conduction. In terms of dimensionless parameters, the Fourier law of heat conduction can be written as

$$Q_{D_t} = \frac{QD}{A\lambda_1(T_f - T_{b1})} = \left.\frac{\partial T_{D_1}}{\partial \eta}\right|_{\eta=0} + \kappa \left.\frac{\partial T_{D_2}}{\partial \eta}\right|_{\eta=0} \tag{20}$$

where the first and the second terms on the right-hand side represent the heat losses to the caprock and the bedrock, respectively. Thus $Q_{D_t}$ represents the total heat lost from the aquifer to the confining beds.

The heat losses from the aquifer to the caprock and bedrock for a given location away from the fault ($\xi_1 = 0.10$) are shown in Figure 8. At early times there are no heat losses to the caprock or the bedrock because the thermal front has not yet arrived. Later, the heat losses increase to a maximum at $\tau_1 \simeq 0.10$, and then rapidly decrease. At $\tau_1 \simeq 1.0$, the heat losses to the caprock stabilize, but those to the bedrock continue to decrease and eventually become negative (i.e., heat flows from the bedrock into the aquifer) at very large times. This behavior can be readily explained, when Figures 4 and 5 are considered. The heat losses from the aquifer to the caprock stabilize when the constant temperature boundary at $z = D$ is felt (approximately at $\tau_1 = 1.0$) and a steady linear gradient is established. However, owing to the constant temperature boundary at $z = -(B + D)$, a linear steady temperature is only achieved at late times as the bedrock is being heated, and this results in negative heat losses. The total heat losses from the aquifer stabilize at an approximate value of $\simeq 1.0$ at late times.

The total heat losses from the aquifer $Q_{D_t}$ versus dimensionless distance $\xi_1$ at various dimensionless times for two different values of $\theta_1$ are shown in Figures 9–10. The figures show that at early times very large heat losses occur close to the fault (small $\xi_1$). However, the heat flux close to the fault decreases logarithmically with time. It can be shown mathe-

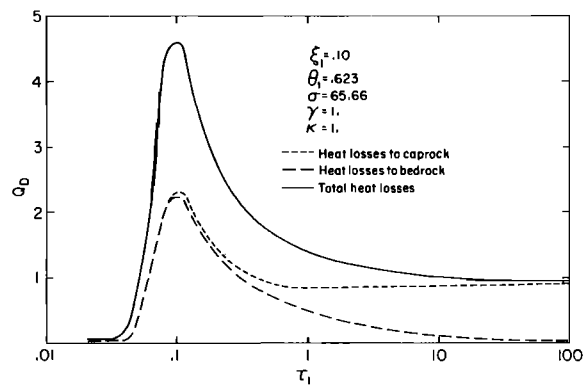


Fig. 8. Dimensionless heat loss ($Q_D$) from the aquifer to the caprock and bedrock.

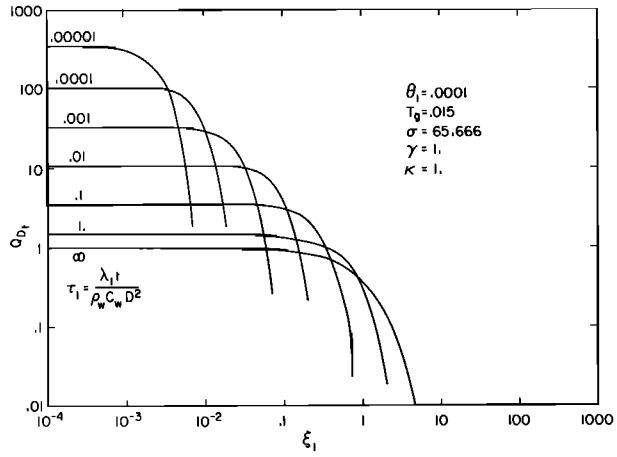


Fig. 9. Total dimensionless heat losses ($Q_{D_1}$) from the aquifer for $\theta_1 = 0.0001$.

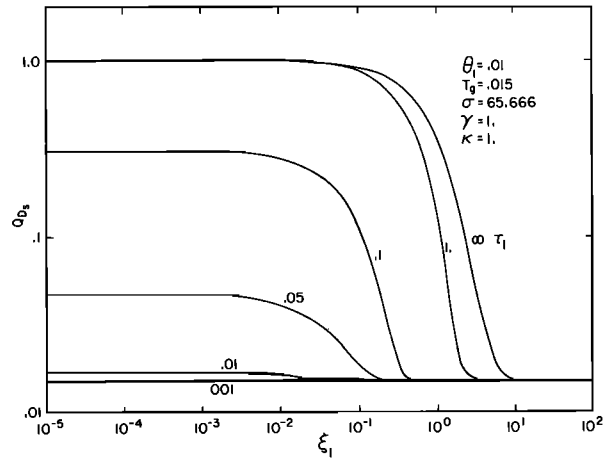


Fig. 11. Heat losses at the ground surface.

matically that the heat losses close to the fault will decrease with time as specified by the following expression [*Carslaw and Jaeger*, 1959]:

$$Q_{D_1} = \frac{2}{\sqrt{\pi \tau_1}} \tag{21}$$

Equation (21) is valid only if $\kappa = \gamma = 1.0$ and at times before the constant-temperature boundary at $z = D$ is felt.

Another interesting characteristic of the curves shown in Figures 9–10 is that they can be enclosed by a single line, representing the area of heat losses at any given dimensionless time $\tau_1$. The reason for this is that the advance of the thermal front along the aquifer is linearly related to dimensionless time. Also, the steady state curves in Figures 9–10 are identical; this again illustrates that the steady state temperature distribution is independent of $\theta_1$. The peculiar maxima in the heat loss curves for large values of $\theta_1$ (Figure 9) are artifacts created by the numerical inverter. There is no theoretical basis for these maxima. The broken lines show the probable locations of the true curves on Figure 10.

### *Heat Losses at the Surface*

The heat losses at the ground surface can also be calculated by using the Fourier law of heat conduction and by evaluating the derivative at the surface ($z = D$). Figure 11 shows the heat losses at the surface versus distance from the fault ($\xi_1$) for a given set of parameters. It may be seen that the thermal front reaches the surface close to the fault at a dimensionless time of about $\tau_1 = 0.001$. Heat flux at the surface increases with dimensionless time until a steady state value is reached at dimensionless time $\tau_1 > 1.0$. For the particular situation shown in Figure 11, the anomalous heat fluxes at the surface due to the fault-charged aquifer beneath extend to a dimensionless distance of approximately $\xi_1 = 10$. Further away from the fault, the heat losses are controlled by the normal geothermal gradient.

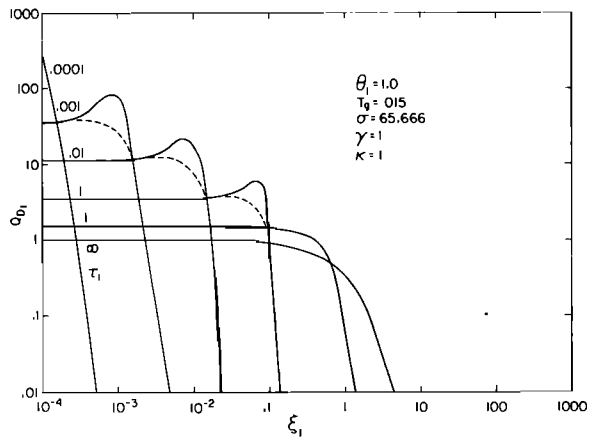


Fig. 10. Total dimensionless heat losses from the aquifer for $\theta_1 = 1.0$.

### *Steady State Conditions*

Equations (16)–(18) give the steady state temperatures in the aquifer, caprock, and bedrock. Figure 12 shows the steady state temperature distribution in the aquifer for various values of $\kappa/\sigma$. Note that the smaller the value of $\kappa/\sigma$, the further away from the fault the thermal field extends. The parameter $\kappa/\sigma$ is a measure of heat losses to the bedrock, with high values indicating either that the thermal conductivity of the bedrock is high or that the constant-temperature boundary beneath the aquifer is close (small value of $B$).

The steady state heat losses from the aquifer can easily be derived from equations (16)–(18), and is given by (see Appendix 2):

$$Q_{D_1} = [1 - T_g]\left[1 + \frac{\kappa}{\sigma}\right] \exp - \left[1 + \frac{\kappa}{\sigma}\right] \xi_1 + T_g(\omega - 1) \tag{22}$$

Heat losses from the aquifer as a function of distance from the fault are shown in Figure 13 for various values of $\sigma$. For this calculation, the geothermal gradient was specified as zero and $\kappa$ was fixed at 1.0. The figure shows that the lower the value of $\sigma$, the higher the heat losses close to the fault and the shorter the extent of the thermal field from the fault. This behavior is reasonable as $\sigma$ is inversely related to the steady loss of heat to the bedrock. For very large values of $\sigma$, the heat losses to the bedrock are negligible and consequently the total heat loss is simply controlled by the heat flux at the ground surface.

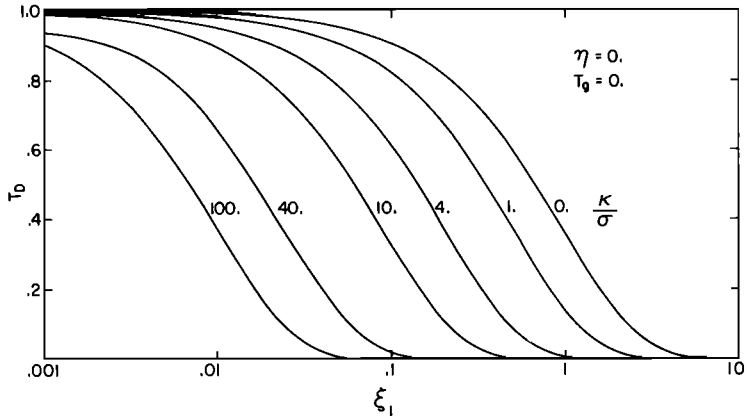


Fig. 12. Steady state temperature distribution in the aquifer for various values of $\kappa/\sigma$.

## APPLICATION TO SUSANVILLE GEOTHERMAL PROJECT

As a first attempt to validate this model for fault-charged hydrothermal systems, it was applied to data from the geothermal system at Susanville, California. The more than 20 exploration wells in Susanville have located a low-temperature (<80°C), shallow geothermal aquifer of limited areal extent [*Benson et al.*, 1981]. Figure 14 shows the location of the wells and the temperature contours at an elevation of 1150 m, which corresponds to a depth of 125 m, where the primary aquifer is found. The temperature contours shown in Figure 14 suggest that the reservoir is charged by a fault with a NW strike; the fault being located slightly west of a line intersecting well S-9 and the Davis well. The steep temperature gradients to the west of the proposed fault illustrate that it is recharging the aquifer only to the east. Temperature contour maps at different depths show fault-related characteristics similar to those shown in Figure 14. Furthermore, many of the wells at Susanville show a reversal with depth as shown in Figure 1.

One potential use for the hydrothermal energy at Susanville is space heating. However, the limited areal extent of the hydrothermal system (Figure 14) indicates that the mass of hot water (the limiting temperature taken as 60°C) amounts to only 1–3 × $10^7$ $m^3$ (depending upon the aquifer thickness selected). Current plans [*U.S. Department of Energy*, 1980] call for an extraction rate of approximately 0.035 $m^3/s$ (550 gpm) for space heating of 14 public buildings. If recharge is neglected, this corresponds to a lifetime of 9–27 years. If the project is intended for 20 years, its success will depend greatly upon the recharge rate. A reliable estimate of the recharge into the Susanville hydrothermal system is therefore of considerable economic interest. Application of our model to the Susanville anomaly can give the first estimate of the recharge rate.

Table 1 shows the parameters selected from the well data. The maximum temperature measured in the field is approximately 80°C in well S-9, which is located very close to the proposed fault (see Figure 14). The temperature of the water recharging the aquifer is therefore fixed at 80°C. Picking 60°C as the average aquifer temperature, the fluid parameters can be obtained, $\rho_w$ = 983 kg/$m^3$, $c_w$ = 4179 J/kg °C. It is now possible to determine that the appropriate value of $\theta_1$ = 0.31 (equation (6c)).

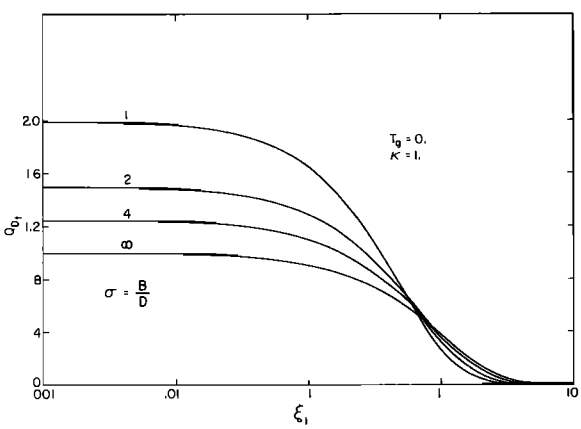


Fig. 13. Steady state heat losses from the aquifer for various values of $\sigma$.

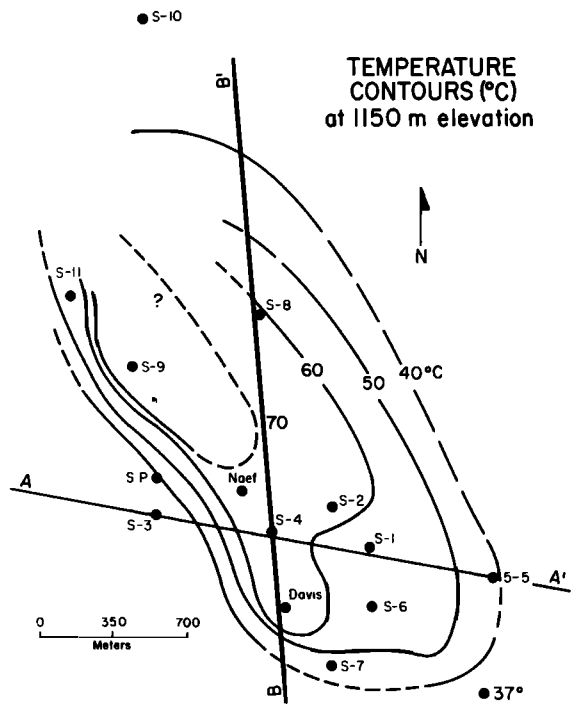


Fig. 14. Temperature contours at 1150 m elevation at Susanville [after *Benson et al.*, 1981].

TABLE 1. Parameters Used for the Susanville Model

| Parameter | Value |
|---|---|
| Aquifer thickness, $b$ | 35 m |
| Depth to aquifer, $D$ | 125 m |
| Aquifer porosity, $\phi$ | 0.2 |
| Thermal conductivity of rock, $\lambda_1$ | 1.5 J/m s °C |
| Rock heat capacity, $c_1$ | 1000 (J/kg °C) |
| Rock density, $\rho_1$ | 2700 (kg/m$^3$) |

The objective of this exercise is to use the model to match the temperature contour data shown in Figure 14 and the temperature profiles from individual wells in an attempt to estimate the hot water recharge. After a number of computer runs, the match shown in Figures 15 and 16 was obtained. As Figure 15 shows, the calculated temperature contours compare very well with the observed ones in the hottest region of the field, close to the proposed fault. Further away, however, there are large differences between the calculated and the observed temperatures. There are several possible reasons for the discrepancy. First, only limited data are available away from the fault (only wells S-5 and S-10), so that temperature contours are not accurately known. Second, evidence shows that there is a high regional flow of groundwater toward the southeast and that mixing of the colder shallow groundwater with the hot fluids is taking place. Third, the subsurface geology is considerably more complex than can be accounted for by the simple model we have used here. In any case, the model matches the temperature profiles of wells close to the proposed fault very well, as shown in Figure 16.

The match shown in Figures 15 and 16 was obtained by

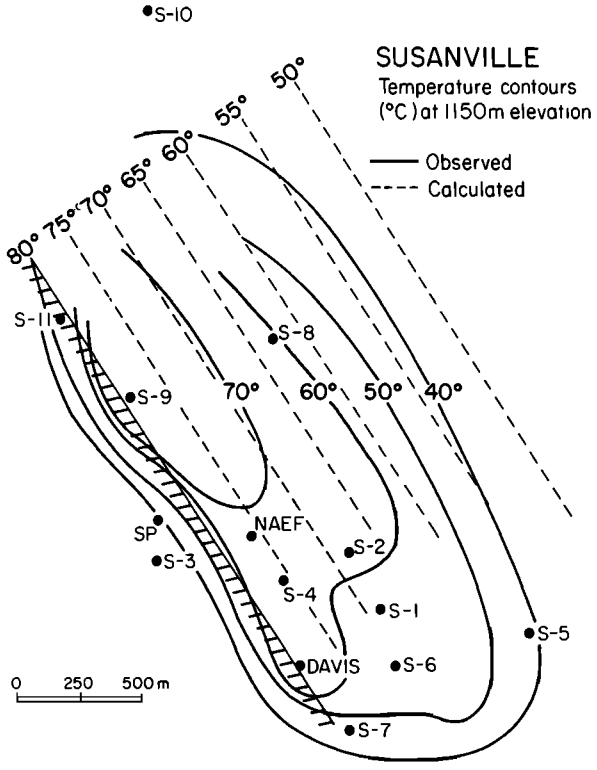


Fig. 15. Comparison between observed and calculated temperature contour data.

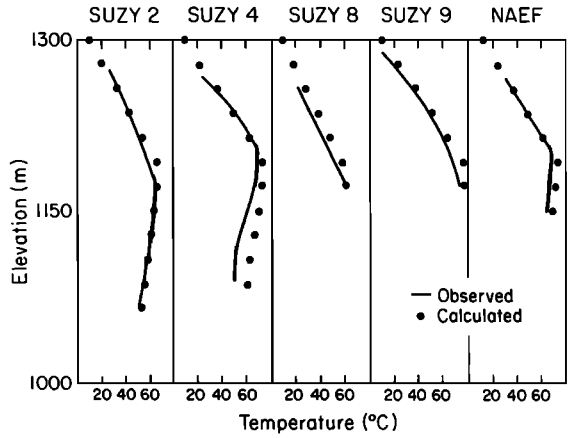


Fig. 16. Comparison between calculated and observed temperature profiles in wells.

using two different sets of parameters. First, if the lower constant temperature boundary is placed very deep ($H \gg D$), the parameters obtained indicate that the hydrothermal system has been under development approximately 2000 years and that the fault charges the system at a rate of $9 \times 10^{-6}$ m$^3$/s m. Second, a very similar match is obtained if the constant temperature boundary is placed at a depth of about 400 m ($\sigma = 2.0$); in this case the parameters obtained show that steady state temperature conditions are reached (consequently the evolution time cannot be determined except that it exceeds 10,000 years) but the calculated recharge rate is the same as in the first case ($9 \times 10^{-6}$ m$^3$/s m). If one considers the age of the subsurface formations at Susanville, the second case seems more likely. Also it is not unlikely that a deeper permeable aquifer with circulation of colder water is present at the site, and this would act as a constant temperature boundary.

Anyway, the accuracy of the calculated recharge rate is of more concern to the developers of the Susanville hydrothermal system than the time of evolution. If the heat losses from the aquifer are controlled by heat conduction as we have assumed in the present model, the calculated recharge rate should be reasonably accurate. However, in the model, horizontal conduction is neglected, and this may make the actual recharge rate greater than what we have calculated.

If we assume that the calculated recharge rate is correct and that the fault recharges over a distance of 2500 m, the total rate of recharge is approximately 0.0225 m$^3$/s. This recharge rate corresponds to approximately 70% of the proposed extraction rate; consequently, a project lifetime of 25–75 years could be expected, or approximately 3 times the longevity if no recharge is considered. It should be emphasized, however, that the simplicity of the present model does not warrant definite conclusions. The results presented here should be considered as rough first estimates.

Unfortunately, detailed heat flow data over the Susanville anomaly are not available at present; such data would have been useful in confirming the accuracy of the model. Figure 17 shows the calculated heat flow values plotted against distance from the proposed fault.

## CONCLUSIONS

A two-dimensional model for fault-charged hydrothermal systems has been developed and used in theoretical studies.

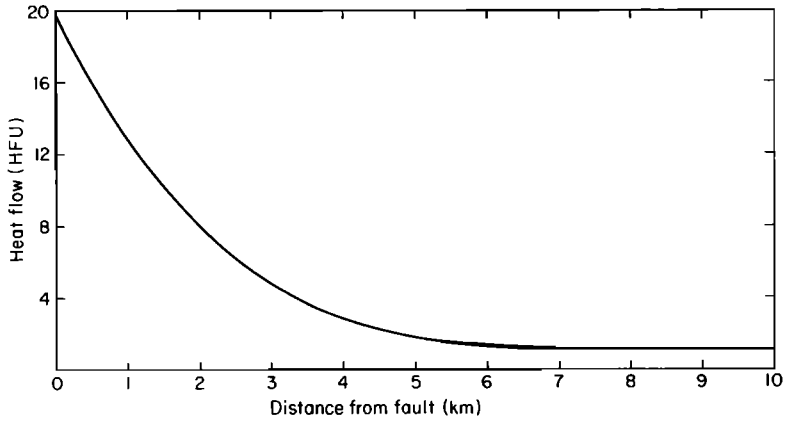


Fig. 17. Calculated heat flows at Susanville.

The physical model used considers a vertical fault recharging hot water to a horizontal aquifer, thereby causing a temperature reversal with depth. The results obtained indicate that the evolution of the thermal field is greatly dependent on $\theta_1$, a parameter denoting the ratio of the heat capacity of the aquifer to that of the caprock. The lower the value of $\theta_1$, the greater the heat losses from the aquifer to the caprock and bedrock. A steady state thermal field in the caprock is established at dimensionless time of $\tau_1$ = 1–10. The steady state temperature field is greatly dependent on the distance to the constant temperature boundary condition at the ground surface ($z = D$). The constant temperature boundary condition below the bedrock ($z = -(D + B)$) exerts a negligible effect, as long as the bedrock is much thicker than the caprock ($D \ll B$). Consequently, the heat losses from the aquifer are primarily governed by the constant temperature condition at the ground surface.

Application of the model to temperature data from wells at Susanville, California, is illustrated. The model is used to match temperature profiles from individual wells as well as temperature contours at the depth of the primary aquifer at Susanville. The results indicate that a fault is recharging the system at a rate of $9 \times 10^{-6}$ m$^3$/s m. As the recharge rate is quite significant, this may increase the potential of the Susanville prospect by a factor of 3.

## APPENDIX 1: SOLUTION OF GOVERNING EQUATIONS

In dimensionless form, the equations governing the temperature in the aquifer, caprock, and bedrock are

$$\eta = 0: \left.\frac{\partial T_{D_1}}{\partial \eta}\right|_{\eta=0} - \kappa \left.\frac{\partial T_{D_2}}{\partial \eta}\right|_{\eta=0} - \frac{\partial T_{D_a}}{\partial \xi_1} - \theta_1 \frac{\partial T_{D_a}}{\partial \tau_1} = 0 \tag{A1}$$

$$\eta > 0: \frac{\partial^2 T_{D_1}}{\partial \eta^2} = \frac{\partial T_{D_1}}{\partial \tau_1} \tag{A2}$$

$$\eta < 0: \frac{\partial^2 T_{D_2}}{\partial \eta^2} = \frac{\gamma}{\kappa} \frac{\partial T_{D_2}}{\partial \tau_1} \tag{A3}$$

The initial conditions are

$$T_{D_a}(\xi_1, 0) = T_g \tag{A4}$$

$$T_{D_1}(\xi_1, \eta, 0) = -T_g(\eta - 1) \tag{A5}$$

$$T_{D_2}(\xi_1, \eta, 0) = -T_g(\omega\eta - 1) \tag{A6}$$

The boundary conditions are

$$T_{D_a}(0, \tau_1) = \begin{cases} 0 & \tau < 0 \\ 1 & \tau \geq 0 \end{cases} \tag{A7}$$

$$T_{D_a}(\xi_1, \tau_1) = T_{D_1}(\xi_1, 0, \tau_1) = T_{D_2}(\xi_1, 0, \tau_1) \tag{A8}$$

$$T_{D_1}(\xi_1, 1, \tau_1) = 0 \tag{A9}$$

$$T_{D_2}(\xi_1, -\sigma, \tau_1) = T_g(\omega\sigma + 1) \tag{A10}$$

After applying Laplace transformation with respect to $\tau_1$, equations (A1)–(A3) become

$$\eta = 0: \left.\frac{\partial v_1}{\partial \eta}\right|_{\eta=0} - \kappa \left.\frac{\partial v_2}{\partial \eta}\right|_{\eta=0} - \frac{\partial u_a}{\partial \xi_1} - \theta_1 p u_a + \theta_1 T_g = 0 \tag{A11}$$

$$\eta > 0: \frac{\partial^2 v_1}{\partial \eta^2} - p v_1 - T_g(\eta - 1) = 0 \tag{A12}$$

$$\eta < 0: \frac{\partial^2 v_2}{\partial \eta^2} - q v_2 - T_g(\omega\eta - 1) = 0 \tag{A13}$$

where $q$ is defined as $q = (\gamma/\kappa)p$. The boundary conditions become

$$u_a(0) = \frac{1}{p} \tag{A14}$$

$$u_a(\xi_1) = v_1(\xi_1, 0) = v_2(\xi_1, 0) \tag{A15}$$

$$v_1(\xi_1, 1) = 0 \tag{A16}$$

$$v_2(\xi_1, -\sigma) = \frac{T_g}{p}(\omega\sigma + 1) \tag{A17}$$

Equations (A12) and (A13) are nonhomogeneous second-order ordinary differential equations. The general form of the equations for a dependent variable $y$ is

$$\frac{\partial^2 y}{\partial \eta^2} - p y = T_g(\eta - 1) \tag{A18}$$

To solve equation (A18), one must obtain a solution to the homogeneous equation ($y_c$) and a particular solution to the nonhomogeneous equation ($y_p$). The complete solution is then

$$y = y_c + y_p \tag{A19}$$

The solution to the homogeneous equation is simply

$$Y_c = A \cosh \sqrt{p}\,\eta + B \sinh \sqrt{p}\,\eta \tag{A20}$$

where $A$ and $B$ are constants. Now we guess a solution to the nonhomogeneous equation as

$$y_p = C\eta + D \tag{A21}$$

where $C$ and $D$ are constants. Substituting equation (A21) into equation (A18) and equating the coefficients yields

$$C = -\frac{T_g}{p} \tag{A22}$$

$$D = \frac{T_g}{p} \tag{A23}$$

The complete solution to equation (A18) can now be written as

$$y = A \cosh \sqrt{p}\,\eta + B \sinh \sqrt{p}\,\eta - \frac{T_g}{p}(\eta - 1) \tag{A24}$$

After obtaining a solution for equation (A18), the solutions for equations (A12) and (A13) are

$$\eta > 0\text{: } v_1 = a_1 \cosh \sqrt{p}\,\eta + b_1 \sinh \sqrt{p}\,\eta - \frac{T_g}{p}(\eta - 1) \tag{A25}$$

$$\eta < 0\text{: } v_2 = a_2 \cosh \sqrt{q}\,\eta + b_2 \sinh \sqrt{q}\,\eta - \frac{T_g}{p}(\omega\eta - 1) \tag{A26}$$

where $a_1$, $a_2$, $b_1$, $b_2$ are constants. Applying boundary condition given by equation (A15) yields

$$a_1 = a_2 = u_a - \frac{T_g}{p} \tag{A27}$$

Similarily, the boundary conditions given by equations (A16) and (A17) can be used to determine $b_1$ and $b_2$

$$b_1 = -\frac{[u_a - (T_g/p)]}{\tanh \sqrt{p}} \tag{A28}$$

$$b_2 = \frac{[u_a - (T_g/p)]}{\tanh \sqrt{q}\,\sigma} \tag{A29}$$

Substituting equations (A27)–(A29) into equations (A25) and (A26) yields

$$\eta > 0\text{: } v_1 = \left[u_a - \frac{T_g}{p}\right]\left\{\cosh \sqrt{p}\,\eta - \frac{\sinh \sqrt{p}\,\eta}{\tanh \sqrt{p}}\right\} - \frac{T_g}{p}(\eta - 1) \tag{A30}$$

$$\eta < 0\text{: } v_2 = \left[u_a - \frac{T_g}{p}\right]\left\{\cosh \sqrt{q}\,\eta + \frac{\sinh \sqrt{q}\,\eta}{\tanh \sqrt{q}\,\sigma}\right\} - \frac{T_g}{p}(\omega\eta - 1) \tag{A31}$$

Since the equations for the temperature in the caprock and bedrock have been solved in the Laplace domain, one can proceed to solve equation (A11)

$$\left.\frac{\partial v_1}{\partial \eta}\right|_{\eta=0} = -\frac{\sqrt{p}\,[u_a - (T_g/p)]}{\tanh \sqrt{p}} - \frac{T_g}{p} \tag{A32}$$

$$\left.\frac{\partial v_2}{\partial \eta}\right|_{\eta=0} = +\frac{\sqrt{q}\,[u_a - (T_g/p)]}{\tanh \sqrt{q}\,\sigma} - \frac{\omega T_g}{p} \tag{A33}$$

Substitution of equations (A32) and (A33) into equation (A11) and noting that $\kappa\omega = 1$ yields

$$-\frac{\sqrt{p}\,[u_a - (T_g/p)]}{\tanh \sqrt{p}} - \kappa\frac{\sqrt{q}\,[u_a - (T_g/p)]}{\tanh \sqrt{q}\,\sigma} - \frac{\partial u_a}{\partial \xi_1} - \theta_1 p u_a + \theta_1 T_g = 0 \tag{A34}$$

Rearrangement of equation (A34) yields

$$\frac{\partial u_a}{\partial \xi_1} + \left[\theta_1 p + \frac{\sqrt{p}}{\tanh \sqrt{p}} + \kappa\frac{\sqrt{q}}{\tanh \sqrt{q}\,\sigma}\right] u_a - \frac{T_g}{p}\left[\theta_1 p + \frac{\sqrt{p}}{\tanh \sqrt{p}} + \frac{\kappa\sqrt{q}}{\tanh \sqrt{q}\,\sigma}\right] = 0 \tag{A35}$$

Now let us define $\bar{u}$ as

$$\bar{u} = u_a - \frac{T_g}{p} \tag{A36}$$

Substitution of equation (A36) into equation (A35) yields

$$\frac{\partial \bar{u}}{\partial \xi_1} + \left[\theta_1 p + \frac{\sqrt{p}}{\tanh \sqrt{p}} + \frac{\kappa\sqrt{q}}{\tanh \sqrt{q}\,\sigma}\right]\bar{u} = 0 \tag{A37}$$

The solution of equation (A35) is

$$\bar{u} = C_1 \exp -\left[\theta_1 p + \frac{\sqrt{p}}{\tanh \sqrt{p}} + \frac{\kappa\sqrt{q}}{\tanh \sqrt{q}\,\sigma}\right]\xi_1 \tag{A38}$$

where $C_1$ is a constant. Applying equation (A36) in terms of $u_a$ yields

$$u_a = C_1 \exp -\left[\theta_1 p + \frac{\sqrt{p}}{\tanh \sqrt{p}} + \frac{\kappa\sqrt{q}}{\tanh \sqrt{q}\,\sigma}\right]\xi_1 + \frac{T_g}{p} \tag{A39}$$

The constant $C_1$ can now be determined by using the boundary condition given by equation (A14)

$$C_1 = \frac{1}{p}[1 - T_g] \tag{A40}$$

Substitution of equation (A40) into equation (A39) yields

$$u_a = \frac{1}{p}[1 - T_g] \exp - \left[\theta_1 p + \frac{\sqrt{p}}{\tanh \sqrt{p}} + \frac{\kappa\sqrt{q}}{\tanh \sqrt{q}\,\sigma}\right]\xi_1 + \frac{T_g}{p} \quad \text{(A41)}$$

Equation (A41) represents the temperature in the aquifer in the Laplace domain.

## Appendix 2. Asymptotic Solutions

At early times, the solution for the temperature in the Laplace domain is

$$\eta = 0: u_a = \frac{T_g}{p} \quad \text{(A42)}$$

$$\eta > 0: v_1 = -\frac{T_g}{p}[\eta - 1] \quad \text{(A43)}$$

$$\eta < 0: v_2 = -\frac{T_g}{p}[\omega\eta - 1] \quad \text{(A44)}$$

Equations (A42)–(A44) can easily be inverted from the Laplace domain to real space to yield

$$\eta = 0: T_{D_a} = T_g \quad \text{(A45)}$$

$$\eta > 0: T_{D_1} = -T_g(\eta - 1) \quad \text{(A46)}$$

$$\eta < 0: T_{D_2} = -T_g(\omega\eta - 1) \quad \text{(A47)}$$

Equations (A45)–(A47) represent the initial conditions specified in the problem. However, at a slightly later time, the temperature in the aquifer in the Laplace domain is

$$u_a = \frac{1}{p}[1 - T_g] \exp - [\theta_1 p \xi_1] + \frac{T_g}{p} \quad \text{(A48)}$$

Equation (A48) can be inverted to real space to yield

$$T_{D_a} = [1 - T_g]U_1(\tau_1 - \theta_1\xi_1) + T_g \quad \text{(A49)}$$

At late times as $p \to 0$, $\tanh \sqrt{p} \to \sqrt{p}$ and the equations for the temperature in the Laplace domain simplify to

$$\eta = 0: u_a = \frac{1}{p}[1 - T_g] \exp - \left[1 + \frac{\kappa}{\sigma}\right]\xi_1 + \frac{T_g}{p} \quad \text{(A50)}$$

$$\eta > 0: v_1 = \frac{1}{p}[1 - T_g][1 - \eta] \exp - \left[1 + \frac{\kappa}{\sigma}\right]\xi_1 - \frac{T_g}{p}(\eta - 1) \quad \text{(A51)}$$

$$\eta < 0: v_2 = \frac{1}{p}[1 - T_g]\left[1 + \frac{\eta}{\sigma}\right] \exp - \left[1 + \frac{\kappa}{\sigma}\right]\xi_1 - \frac{T_g}{p}(\omega\eta - 1) \quad \text{(A52)}$$

Equations (A50)–(A52) can be inverted to real space to yield

$$\eta = 0: T_{D_a} = [1 - T_g] \exp - \left[1 + \frac{\kappa}{\sigma}\right]\xi_1 + T_g \quad \text{(A53)}$$

$$\eta > 0: T_{D_1} = [1 - T_g][1 - \eta] \exp - \left[1 + \frac{\kappa}{\sigma}\right]\xi_1 - T_g(\eta - 1) \quad \text{(A54)}$$

$$\eta < 0: T_{D_2} = [1 - T_g]\left[1 + \frac{\eta}{\sigma}\right] \exp - \left[1 + \frac{\kappa}{\sigma}\right]\xi_1 - T_g(\omega\eta - 1) \quad \text{(A55)}$$

Equations (A53)–(A55) give the steady state temperature distribution in the aquifer, caprock, and bedrock.

The steady state total heat losses from the aquifer can be calculated by using the Fourier law of heat conduction. In dimensionless form, the equation for the dimensionless total heat losses from the aquifer is

$$Q_{D_t} = \left.\frac{\partial T_{D_1}}{\partial \eta}\right|_{\eta=0} + \kappa \left.\frac{\partial T_{D_2}}{\partial \eta}\right|_{\eta=0} \quad \text{(A56)}$$

Equations (A54) and (A55) can easily be differentiated with respect to $\eta$ and evaluated at $\eta = 0$. Equation (B15) thus becomes

$$Q_{D_t} = -[1 - T_g]\left[1 + \frac{\kappa}{\sigma}\right] \exp - \left[1 + \frac{\kappa}{\sigma}\right]\xi_1 + T_g(\omega - 1) \quad \text{(A57)}$$

## Notation

- $a$ geothermal gradient (°C/m).
- $B$ thickness of bedrock (m).
- $D$ thickness of caprock (m).
- $H$ thickness of aquifer (m).
- $p$ Laplace parameter.
- $\phi$ porosity.
- $q$ the recharge rate ($m^3$/s m).
- $Q_D$ dimensionless heat losses.
- $t$ time (s).
- $T$ temperature (°C).
- $T_{b1}$ temperature at ground surface (°C).
- $T_D$ dimensionless temperature, $T_D = (T - T_{b1})/(T_f - T_{b1})$.
- $T_f$ temperature of recharged water (°C).
- $T_g$ dimensionless geothermal gradient, $T_g = a_1 D/(T_f - T_{b1})$.
- $x$ lateral coordinate (m).
- $z$ vertical coordinate (m).
- $\gamma$ dimensionless heat capacity, $\gamma = \rho_2 c_2/\rho_1 c_1$.
- $\eta$ dimensionless vertical coordinate, $\eta = z/D$.
- $\theta_1$ dimensionless heat capacity, $\theta_1 = (B/D)(\rho_a c_a/\rho_1 c_1)$.
- $\kappa$ dimensionless thermal conductivity, $\kappa = \lambda_2/\lambda_1$.
- $\lambda$ thermal conductivity (J/m s °C).
- $\xi_1$ dimensionless distance from fault, $\xi_1 = \lambda_1 x/p_w c_w q D$.
- $\rho c$ volumetric heat capacity (J/$m^3$ °C).

$\sigma$ dimensionless geometrical factor, $\sigma = B/D$.
$\tau_1$ dimensionless time, $\tau_1 = \lambda_1 t/\rho_1 c_1 D^2$.
$\omega$ ratio of geothermal gradients, $\omega = a_2/a_1$.

*Subscripts*

$a$ aquifer.
1 rock matrix above aquifer.
2 rock matrix below aquifer.
$w$ liquid water.

*Acknowledgments.* The authors express their gratitude to Keshav Goyal and Karsten Pruess for critical review of this manuscript. This work was supported by the Assistant Secretary for Conservation and Renewable Energy, Office of Renewable Technology, Division of Geothermal and Hydropower Technologies, of the U.S. Department of Energy under contract DE-AC03-76SF00098.

## REFERENCES

Benson, S. M., C. B. Goranson, J. Noble, R. Schroeder, D. Corrigan, and H. Wollenberg, Evaluation of the Susanville, California, geothermal resource, *LBL-11187*, Lawrence Berkeley Lab., Berkeley, Calif., 1981.

Bodvarsson, G., Thermal problems in the siting of reinjection wells, *Geothermics, 1*, 2, 1972.

Bodvarsson, G. S., and C. F. Tsang, Injection and thermal breakthrough in fractured geothermal reservoirs, *J. Geophys. Res., 87*, 1031–1048, 1982.

Carslaw, H. S., and J. C. Jaeger, Conduction of heat in solids, Oxford University Press, New York, 1959.

Goyal, K. P., and D. R. Kassoy, Fault zone controlled charging of a liquid-dominated geothermal reservoir, *J. Geophys. Res., 85*, 1867–1875, 1980.

Goyal, K. P., and D. R. Kassoy, A plausible two-dimensional vertical model of the East Mesa geothermal field, California, U.S.A., *J. Geophys. Res., 86*, 10719–10733, 1981.

Goyal, K. P., and T. N. Narasimhan, Heat and mass transfer in a fault-controlled geothermal reservoir charged at constant pressure, *81-HT-52*, Am. Soc. of Mech. Eng., New York, 1981.

Kilty, K., D. S. Chapman, and C. Mase, Aspects of forced convective heat transfer in geothermal systems, *Top. Rep. 78-1701.a.6.4.1*, Univ. of Utah, Salt Lake City, Utah, 1978.

Lauwerier, H. A., The transport of heat in an oil layer caused by the injection of hot fluid, *Appl. Sci. Res.*, Sec. A, *5*, 145, 1955.

Pritchett, J. W., and S. K. Garg, Flow in an aquifer charged with hot water from a fault zone, *Pure Appl. Geophys., 117*, 309–320, 1979.

Riney, T. D., J. W. Pritchett, L. F. Rice, and S. K. Garg, A preliminary model of the East Mesa hydrothermal systems, in Proceedings 5th Workshop in Geothermal Reservoir Engineering, *SGP-TR-40*, Stanford Univ., Stanford, Calif., 1979.

Sorey, M. L., Numerical modeling of liquid geothermal systems, Ph.D. thesis, Univ. of Calif., Berkeley, 1975.

Stehfest, H., Numerical inversion of Laplace transforms, *Communications ACM, 13*, 44–49, 1970.

U.S. Department of Energy, Geothermal direct heat applications, program summary, Report of the Semi-Annual Review Meeting, U.S. Department of Energy, Geothermal Energy Division, Las Vegas, Nevada, 1980.

(Received March 12, 1982;
revised July 12, 1982;
accepted August 13, 1982.)